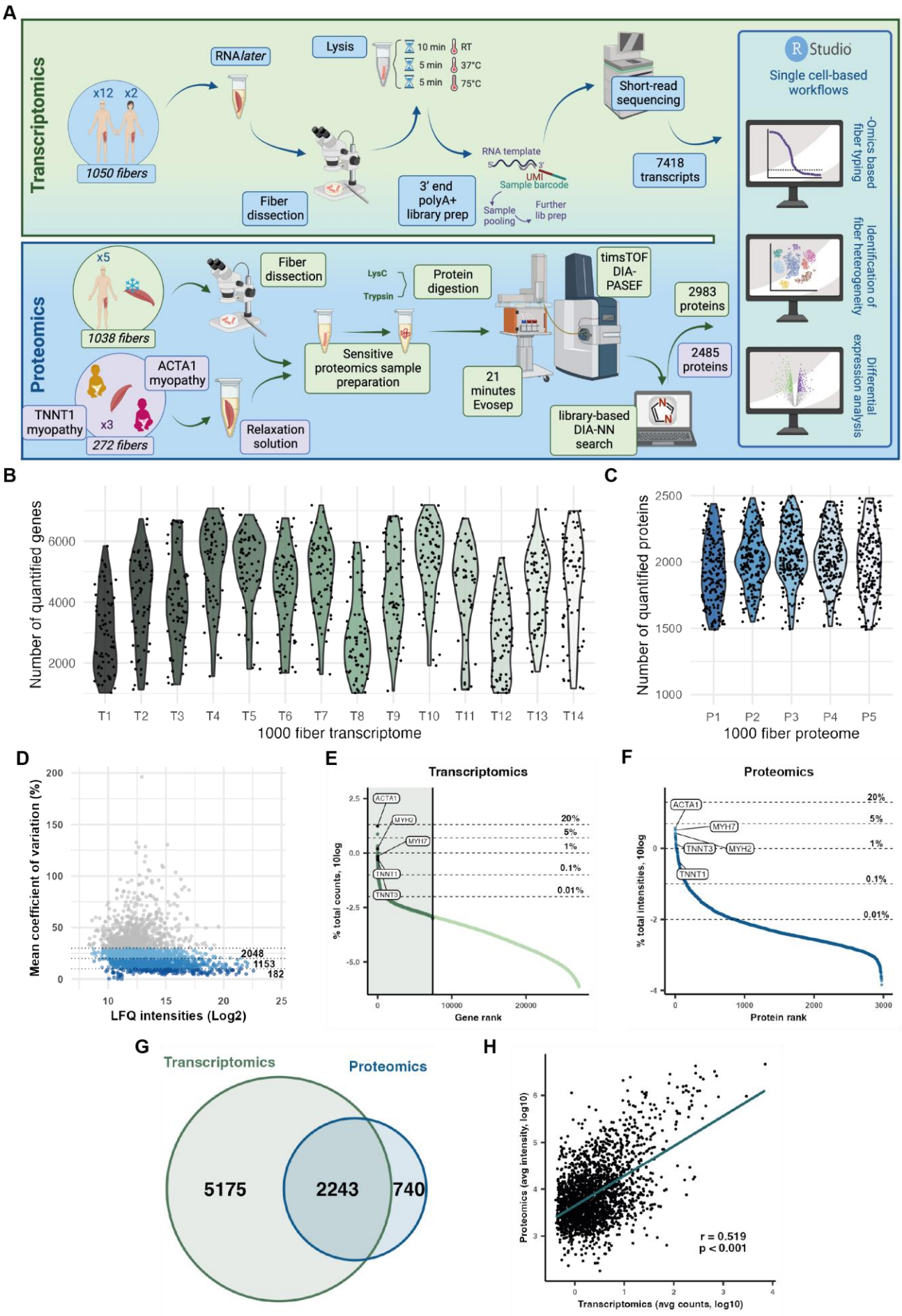

Supplementary Figure 1. **Quality control of novel transcriptomic and proteomic workflows.** (**A**) Detailed schematic of developed workflows (created using BioRender.com). (**B-C**) Number of quantified genes/proteins by participant and sample in 1000 fiber transcriptomics and proteomics. (**D**) Coefficient of variation by protein in 1000 fiber proteomics. (**E-F**) Dynamic range of genes in 1000 fiber transcriptomics and of proteins in 1000 fiber proteomics. (**G**) Overlapping features within 1000 fiber transcriptomics and proteomics. (**H**) Correlation between features within 1000 fiber transcriptomics and proteomics. (n = 14 and n = 5 for all transcriptomics and proteomics, respectively).

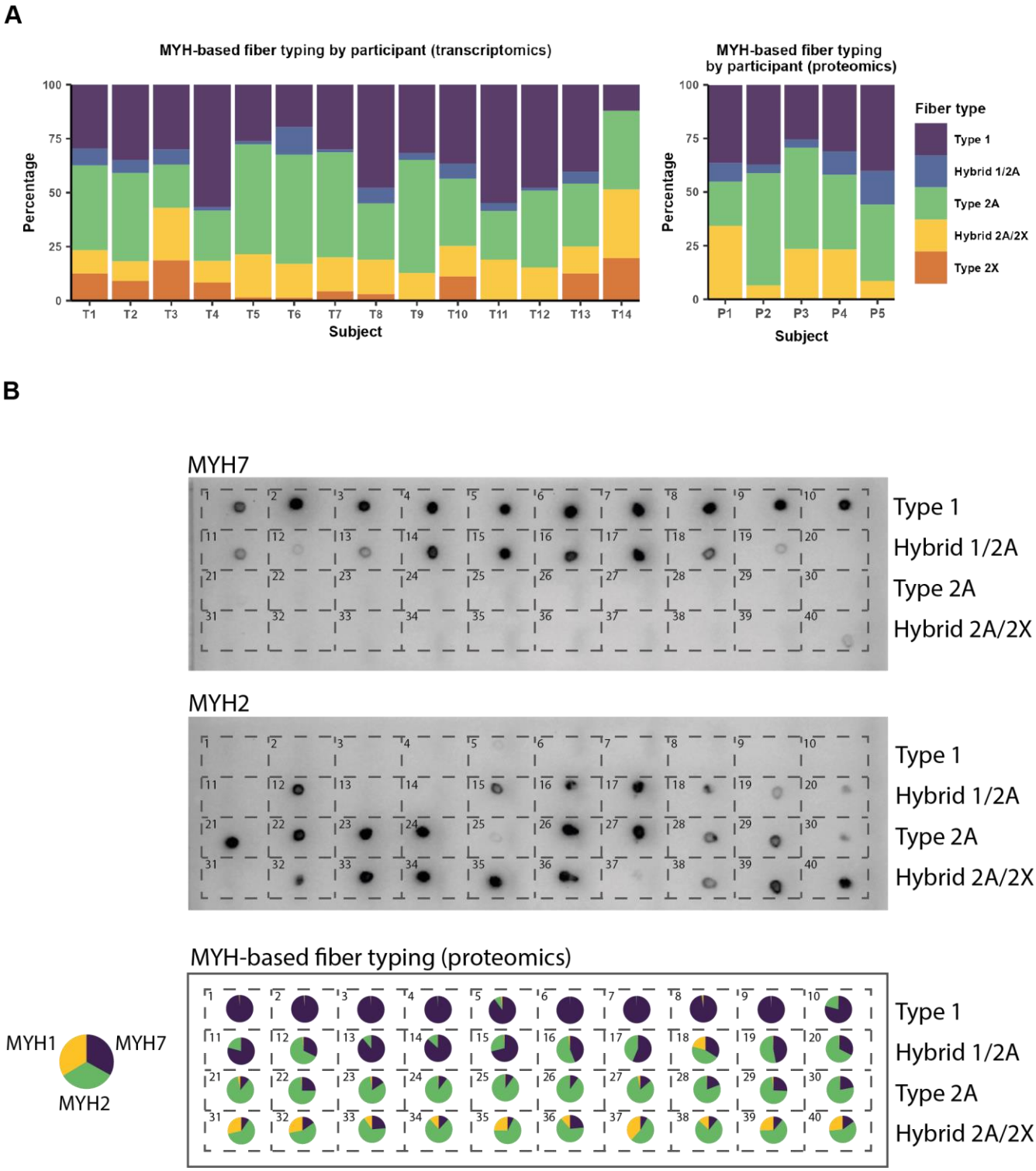

Supplementary Figure 2. Higher sensitivity with proteomics compared to standard dot blotting. (**A**) MYH-based fiber type proportions by participant. (**B**) Comparison between dot blot- and proteomics-based fiber typing. The pie chart indicates the abundance for each MYH isoform in the single-fiber proteomics data.

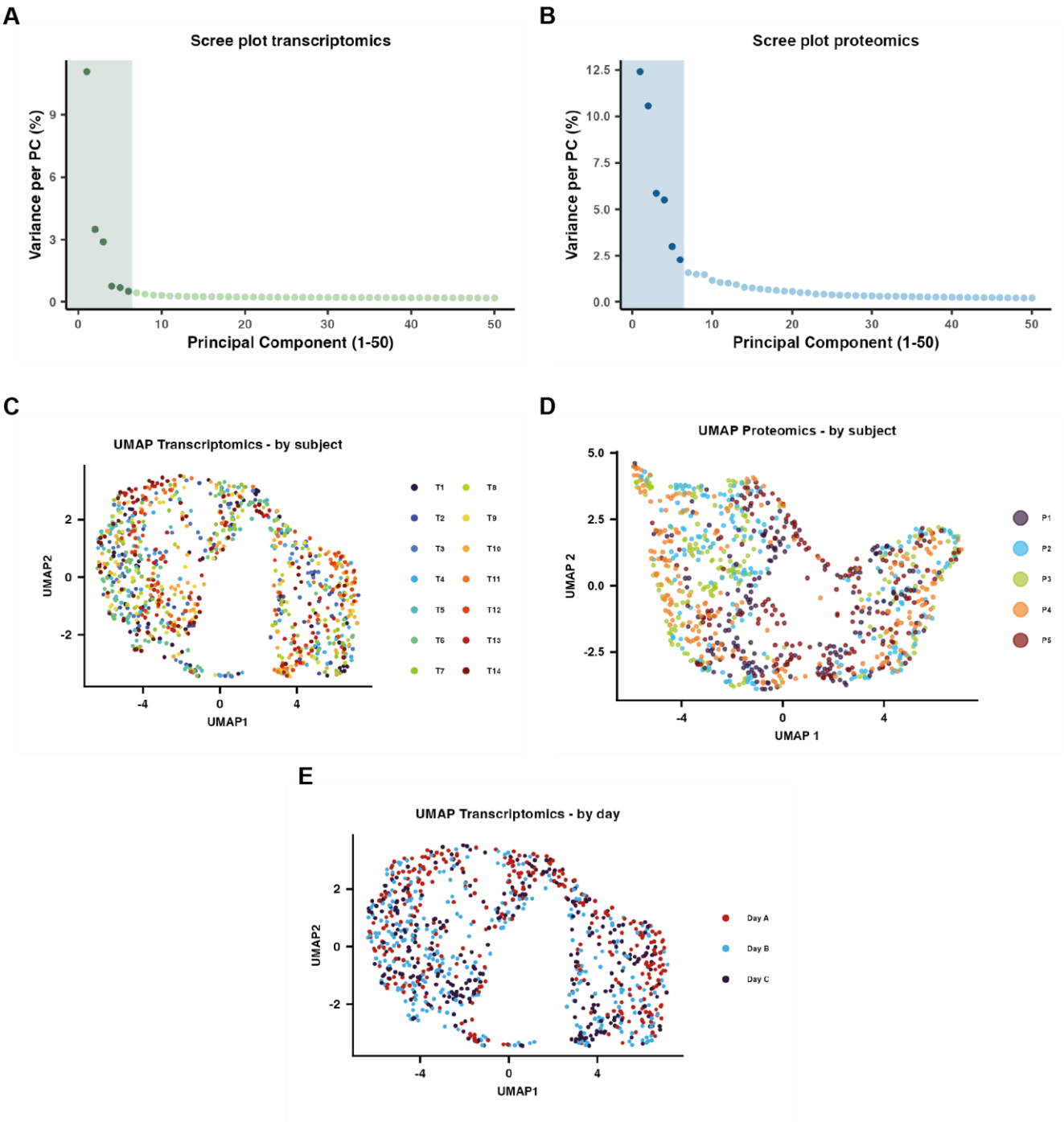

Supplementary Figure 3. Clustering of transcriptomic and proteomic data. (**A-B**) Scree plots of transcriptomics and proteomics. Colored box indicates the number of principal components used for clustering. (**C-D**) 1000 fiber transcriptomics and proteomics UMAP colored by participant. (**E**) 1000 fiber transcriptomics UMAP colored by trial day. (n = 14 and n = 5 for all transcriptomics and proteomics, respectively).

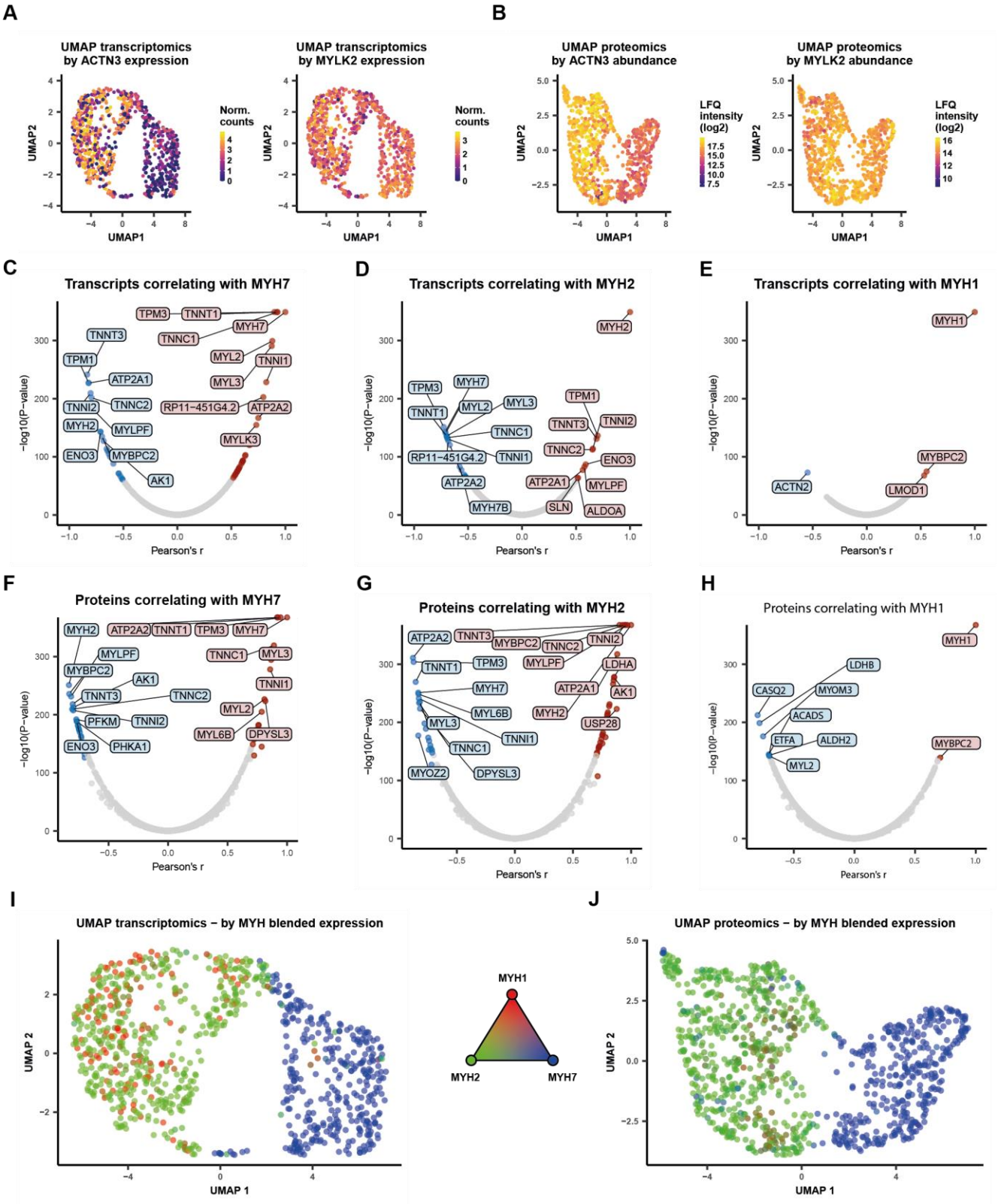

Supplementary Figure 4. Type 2X is not a distinct fiber type. (**A-B**) Feature plots for ACTN3 and MYLK2 expression/abundance in transcriptomics and proteomics data. (**C-H**) U-plots demonstrating correlation (Pearson correlation) of transcripts/proteins with the different MYH isoforms. X-axis depicts Pearson's r coefficient, y-axis depicts -log10 of the p-value. (**I-J**) UMAP plots for transcriptomics and proteomics showing blended expression of MYH7 (blue), MYH2 (green) and MYH1 (red).

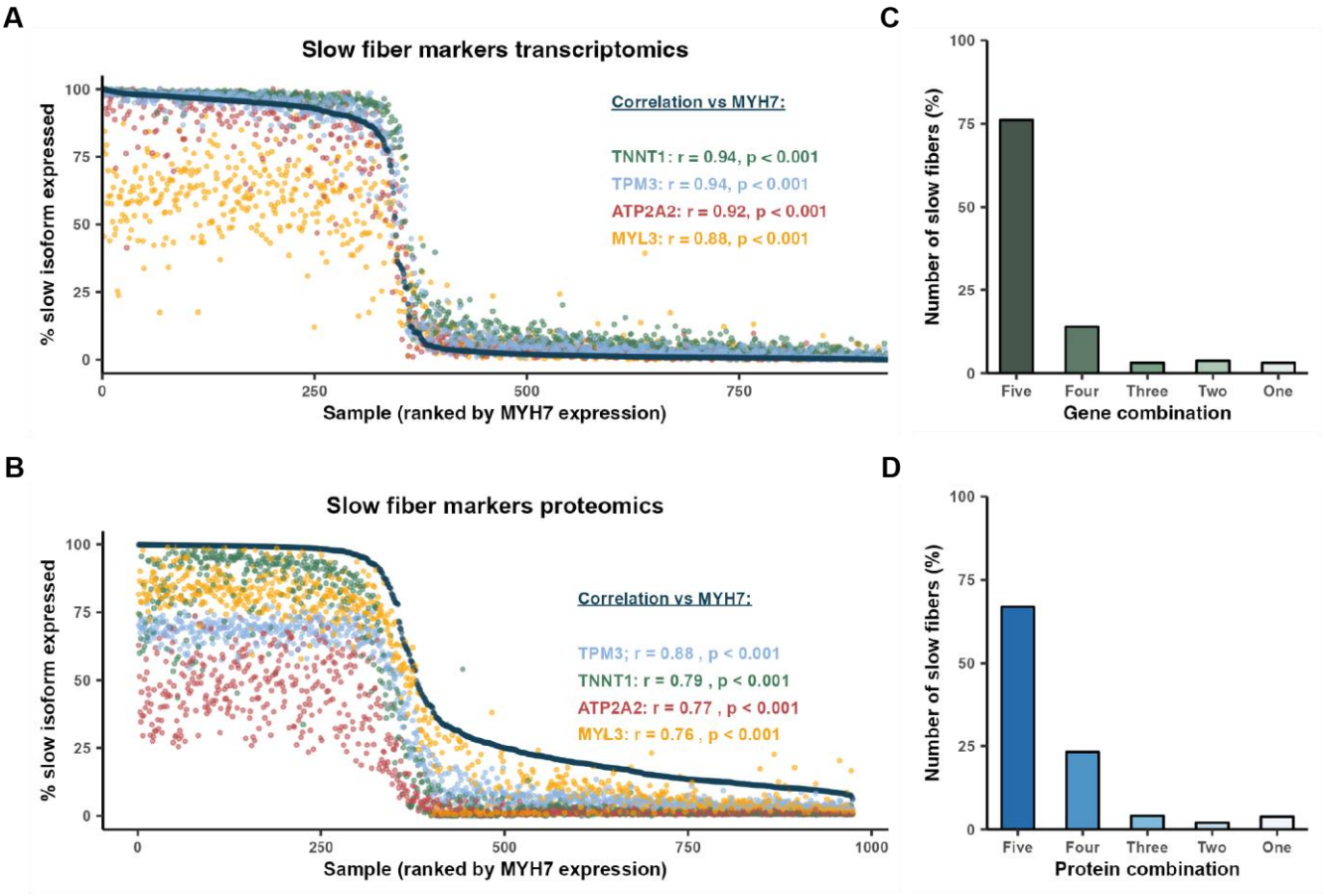

Supplementary Figure 5. Heterogeneity of fibers with well-known fiber type specific features. (**A-B**) Fiber type curves of established slow fiber type genes/proteins in 1000 fiber transcriptomics and proteomics, correlation was determined using Pearson's r. (**C-D**) Proportion of fibers determined to be slow via different numerical combinations of genes/proteins (from A-B) in 1000 fiber transcriptomics and proteomics.

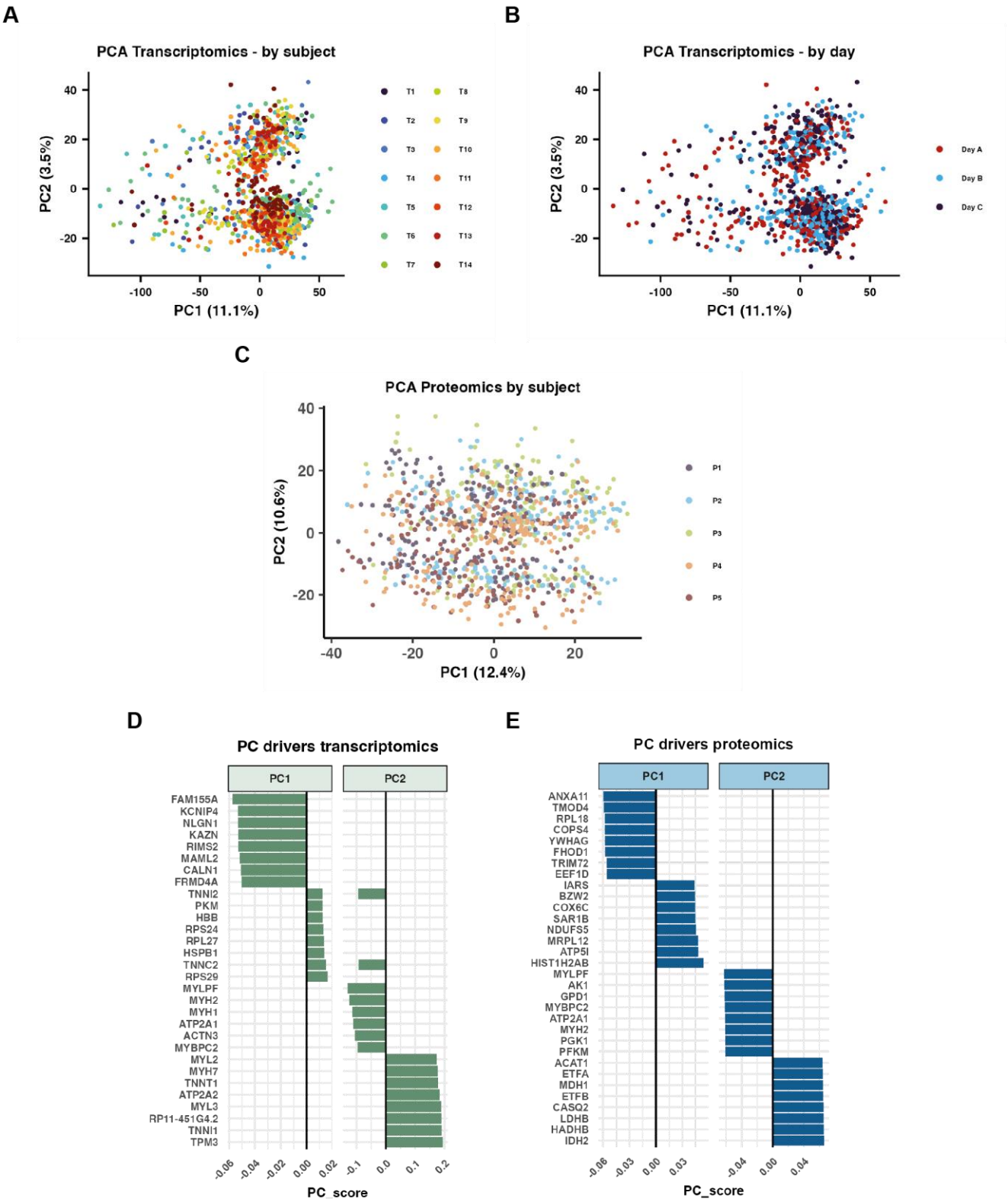

Supplementary Figure 6. Additional data of Principal Component Analysis (PCA). (**A-B**) 1000 fiber transcriptomics PCA plot colored by participant or trial day. (**C**) 1000 fiber proteomics PCA plot colored by participant. (**D-E**) Top gene and protein drivers of PC1 and PC2**.**

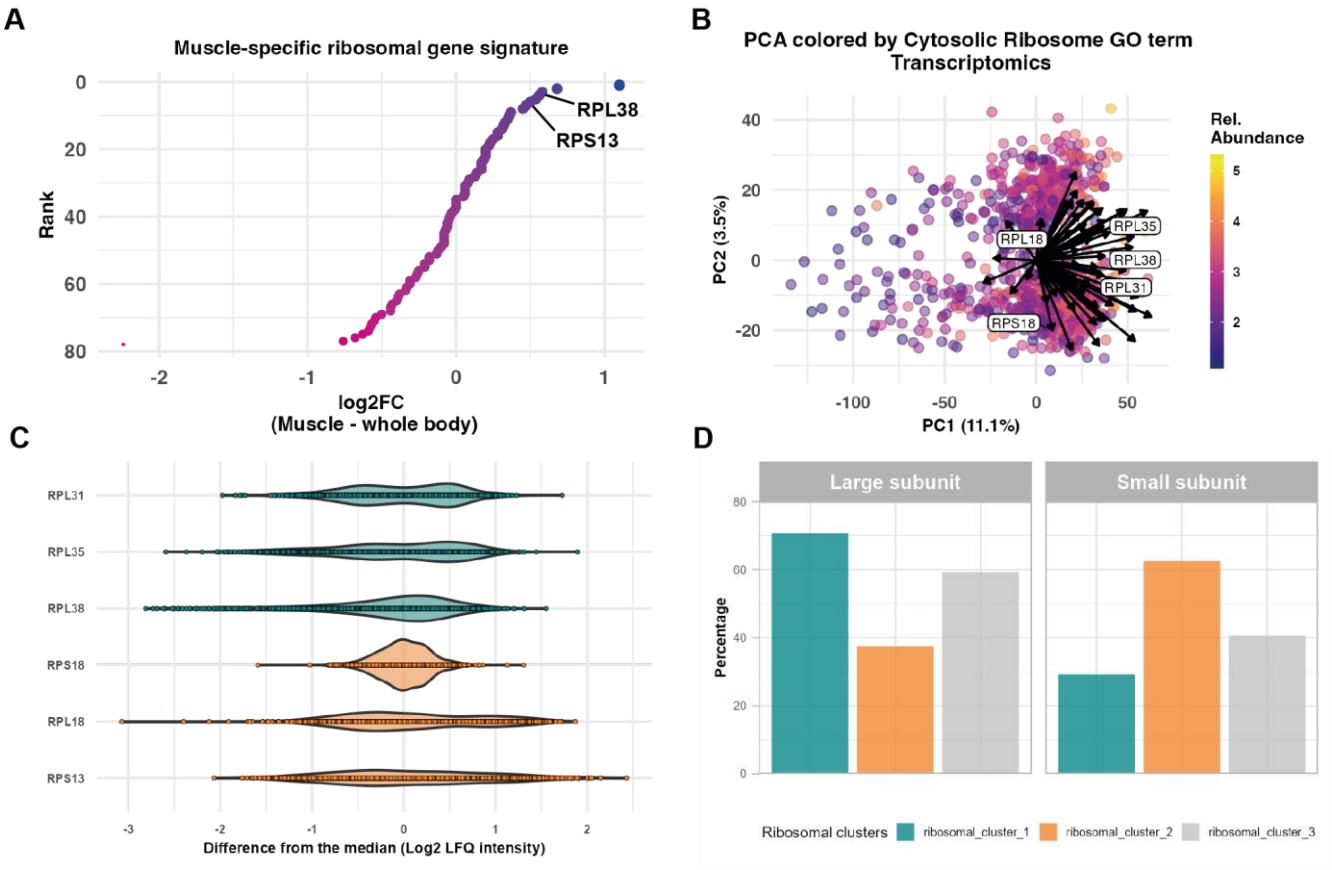

Supplementary Figure 7. Ribosomal heterogeneity of skeletal muscle fibers. (**A**) mRNA expression of ribosomal proteins in skeletal muscle compared to the whole body. Data derived from Panda et al[67]. (**B**) PCA plot colored by cytosolic ribosome gene ontology (GO) term in the transcriptome. Arrows indicate the direction towards which the proteins are driving the variance in the PCA plot. The length of the lines represents the principal component score for a given protein. (**C**) Differences in protein abundance of ribosomal proteins in single muscle fibers compared to the median abundance. (**C**) Proportions of ribosomal proteins in each cluster by small (40S) and large (60S) subunits.

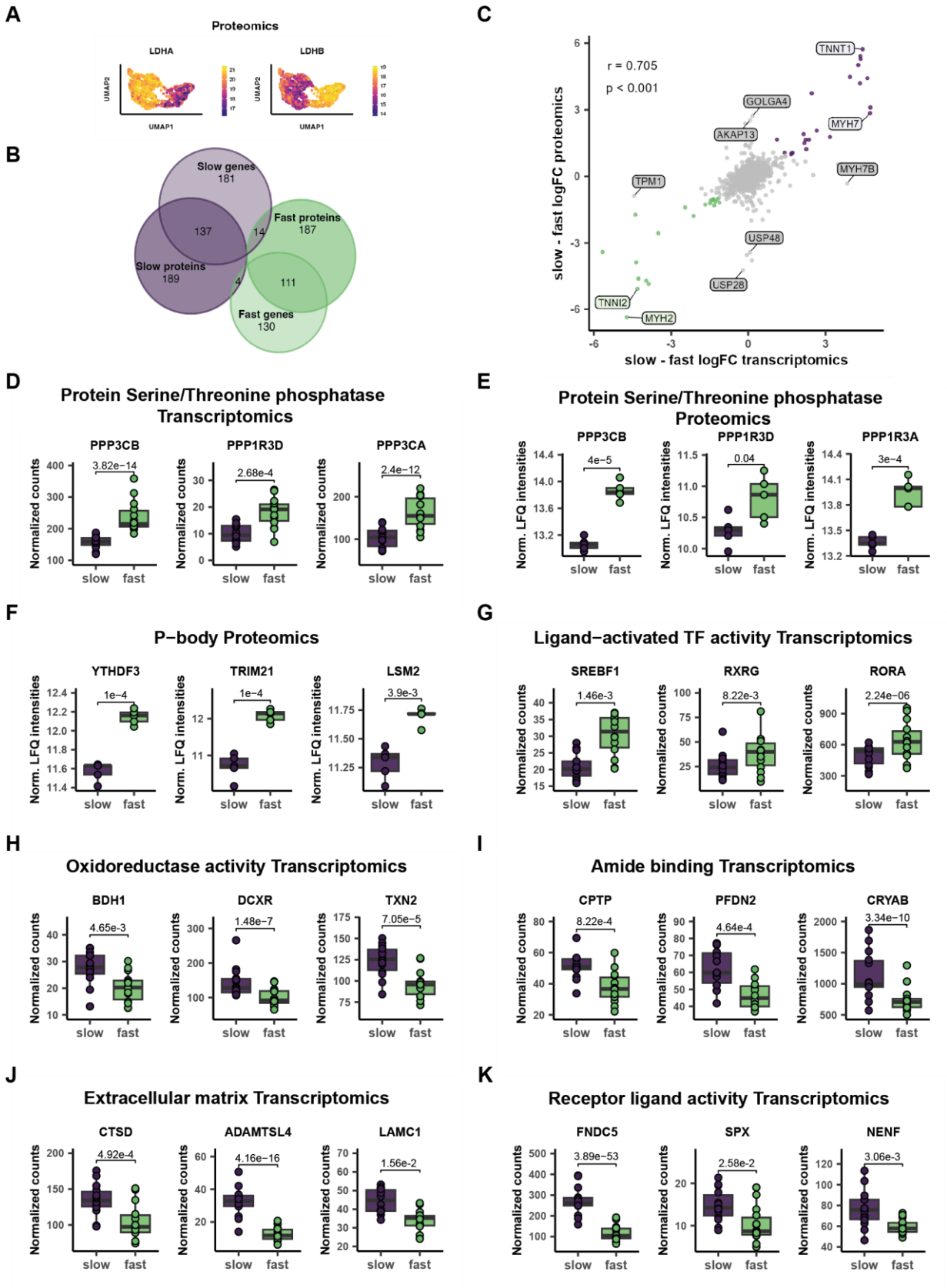

Supplementary Figure 8. Gene and protein signatures of fast and slow fibers. (**A**) Feature plots of LDH protein isoforms between slow and fast fibers. (**B**) Overlap of significantly different genes/proteins between slow and fast skeletal muscle fibers in 1000 fiber transcriptomics and proteomics. (**C**) Pearson correlation between the $\log_2$ fold change difference between slow and fast skeletal muscle fibers within 1000 fiber transcriptomics and proteomics. (**D-K**) Expression profiles of top drivers of selected enrichment terms within slow or fast fibers with indication of adjusted p-values. Benjamini-Hochberg adjusted p values are derived from the DESeq2 Wald test (transcriptomics) or a Limma linear model approach with empirical Bayes methods. Boxplots display the median and first and third quartile, with the whiskers extending towards the largest/smallest values. (n = 14 and n = 5 for all transcriptomics and proteomics, respectively).

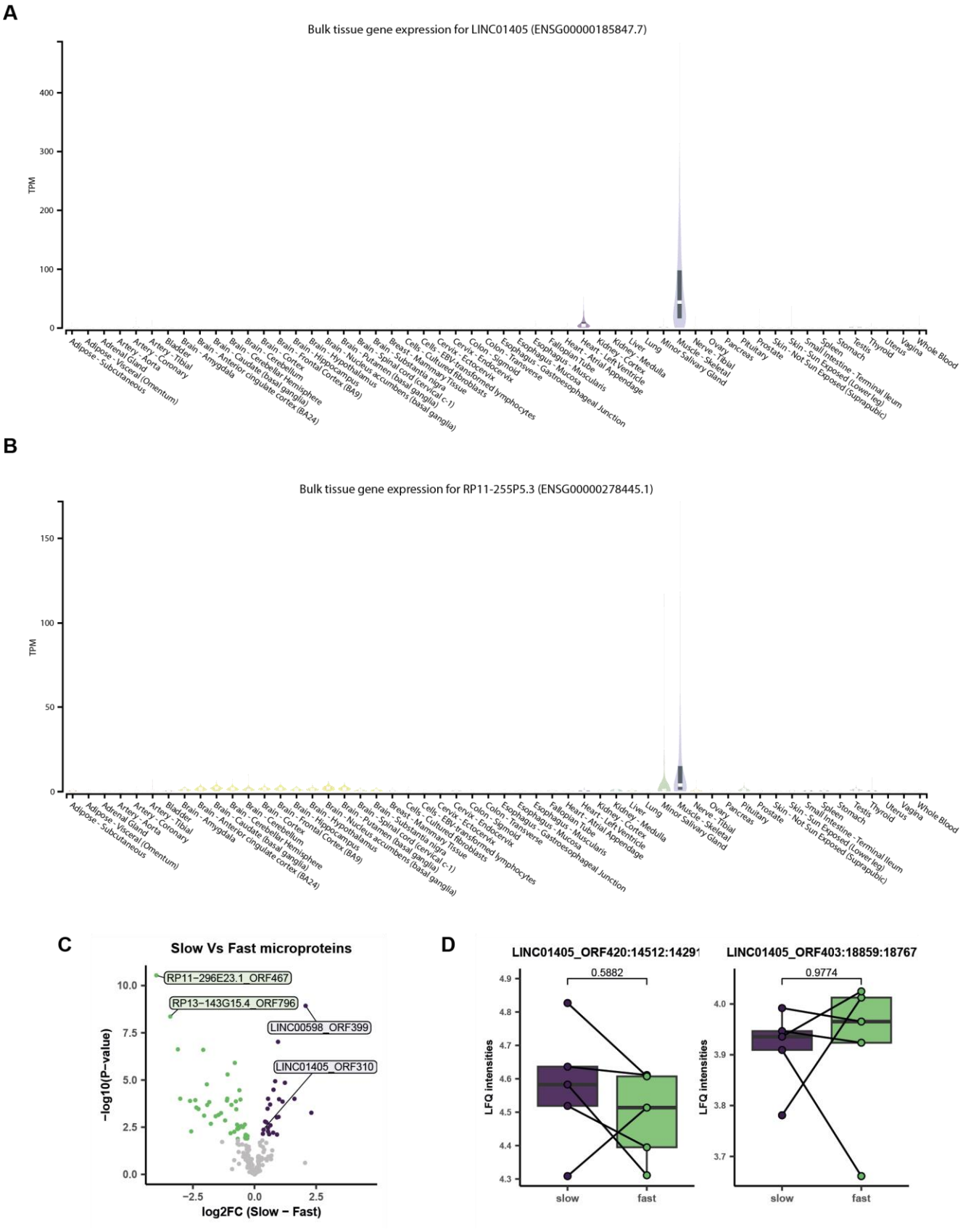

Supplementary Figure 9. Specific expression of non-coding RNA and microproteins in skeletal muscle. (**A-B**) Expression profile of *LINC01405* and *RP11-255P5.3* in different tissues. (**C**) Volcano plots comparing microprotein abundance between the slow and fast clusters identified from the uniform manifold approximation and projection (UMAP) plots in Fig 1G-H. Colored dots represent significantly different microproteins at an FDR < 0.05. **(D)** Slow/fast fiber-type comparison of LINC01405_ORF52 14515:14294 and LINC01405_ORF503 18862:18770 microproteins. Statistical analysis was performed using a Limma linear model approach with empirical Bayes methods followed by p-value adjustment (Benjamini-Hochberg). Boxplots display the median and first and third quartile, with the whiskers extending towards the largest/smallest values. (n = 5 for C and D).

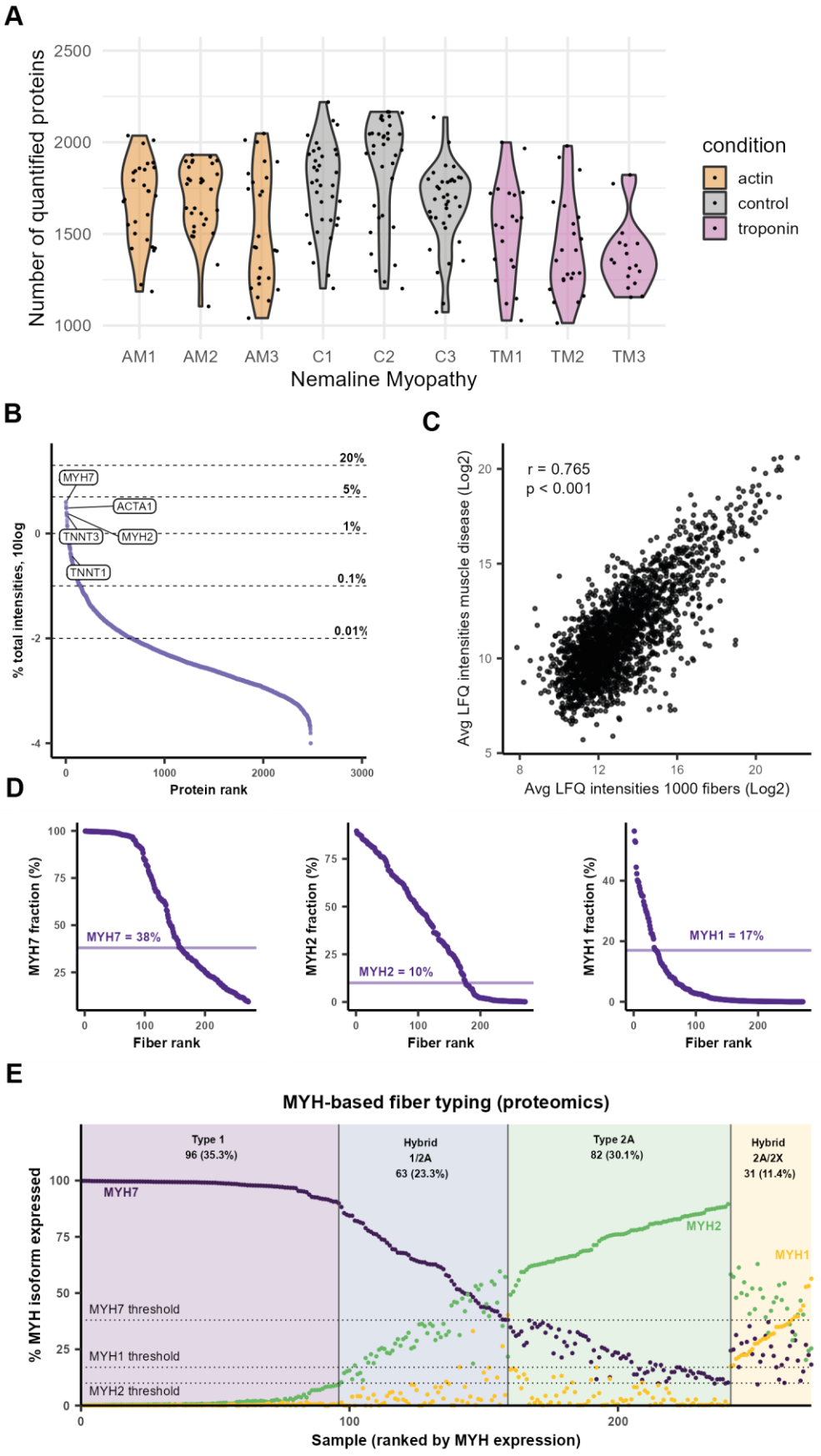

Supplementary Figure 10. Quality control and fiber typing of nemaline myopathy dataset. (**A**) Number of quantified proteins by participant and sample in nemaline myopathy proteomics. (**B**) Dynamic range of proteins in nemaline myopathy proteomics. (**C**) Pearson correlation between features within 1000 fiber proteomics and healthy controls of nemaline myopathy proteomics. (**D**) Dynamic range curves for MYH7, MYH2, and MYH1, with calculated assignment thresholds for fiber typing. (**E**) Distribution of fibers by expression of MYHs in nemaline myopathy proteomics.

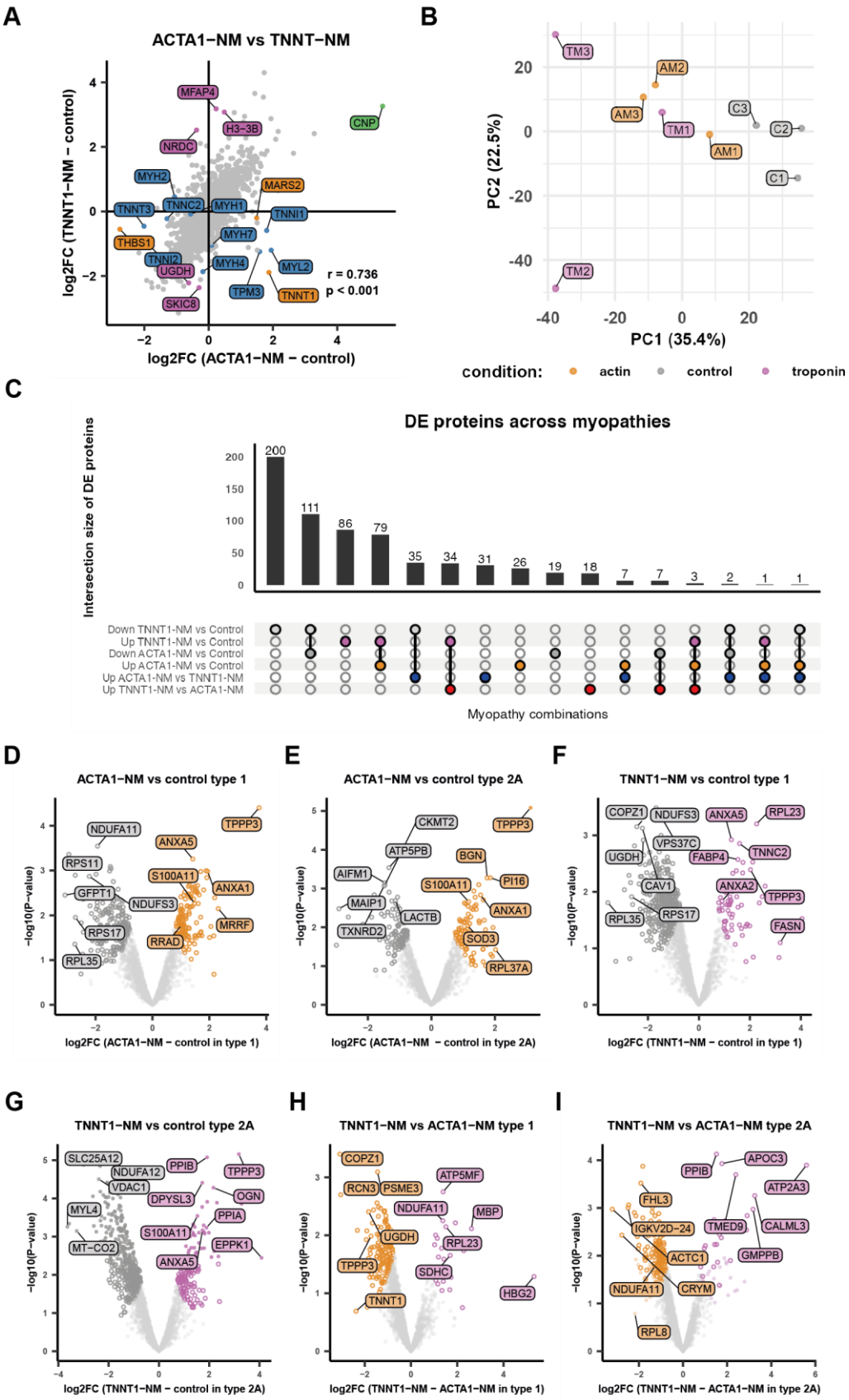

Supplementary Figure 11. Fiber type-independent remodelling in nemaline myopathy. (**A**) Spearman correlation between the $\log_2$ fold change difference between *ACTA1*- and *TNNT1*-nemaline myopathies with control participants (n = 3 for each group). (**B**) PCA of nemaline myopathy patients (pseudobulked protein profile form single fibers). (**C**) Upset plot of significantly regulated proteins *ACTA1*- and *TNNT1*-nemaline myopathies. (**D-I**) Volcano plots comparing the *ACTA1*- and *TNNT1*-nemaline myopathies with control participants and between *ACTA1*- and *TNNT1*-nemaline myopathies by MYH-based fiber type. Colored circles represent significantly different proteins at $\pi < 0.05$, darker dots represent significantly different proteins at FDR < 0.05. Statistical analysis was performed using a Limma linear model approach with empirical Bayes methods followed by p-value adjustment (Benjamini-Hochberg) and Xiao value calculation.

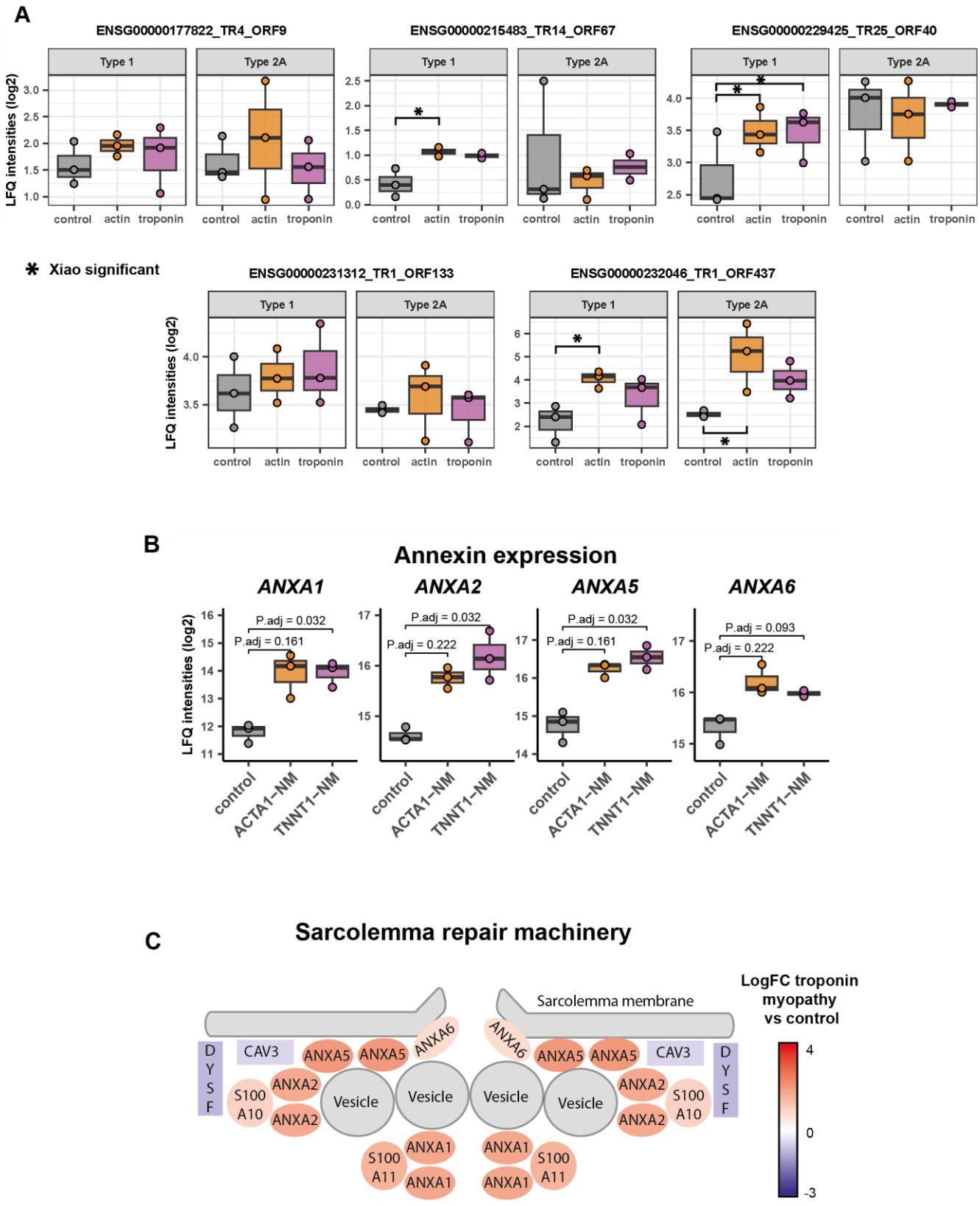

Supplementary Figure 12. Effects of nemaline myopathy on microproteins and the sarcolemma repair machinery. **(A)** Protein abundance of identified microproteins within ACTA1-, TNNT1- and control participants. Significantly different comparisons between groups are highlighted. **(B)** Abundance of annexin proteins in *ACTA1*- and *TNNT1*-nemaline myopathy. (**C**) Schematic of changes within the sarcolemma repair machinery in nemaline myopathy. Boxplots display the median and first and third quartile, with the whiskers extending towards the largest/smallest values. Statistical analysis was performed using a Limma linear model approach with empirical Bayes methods followed by p-value adjustment (Benjamini-Hochberg) and Xiao value calculation. (n = 3 for each group).

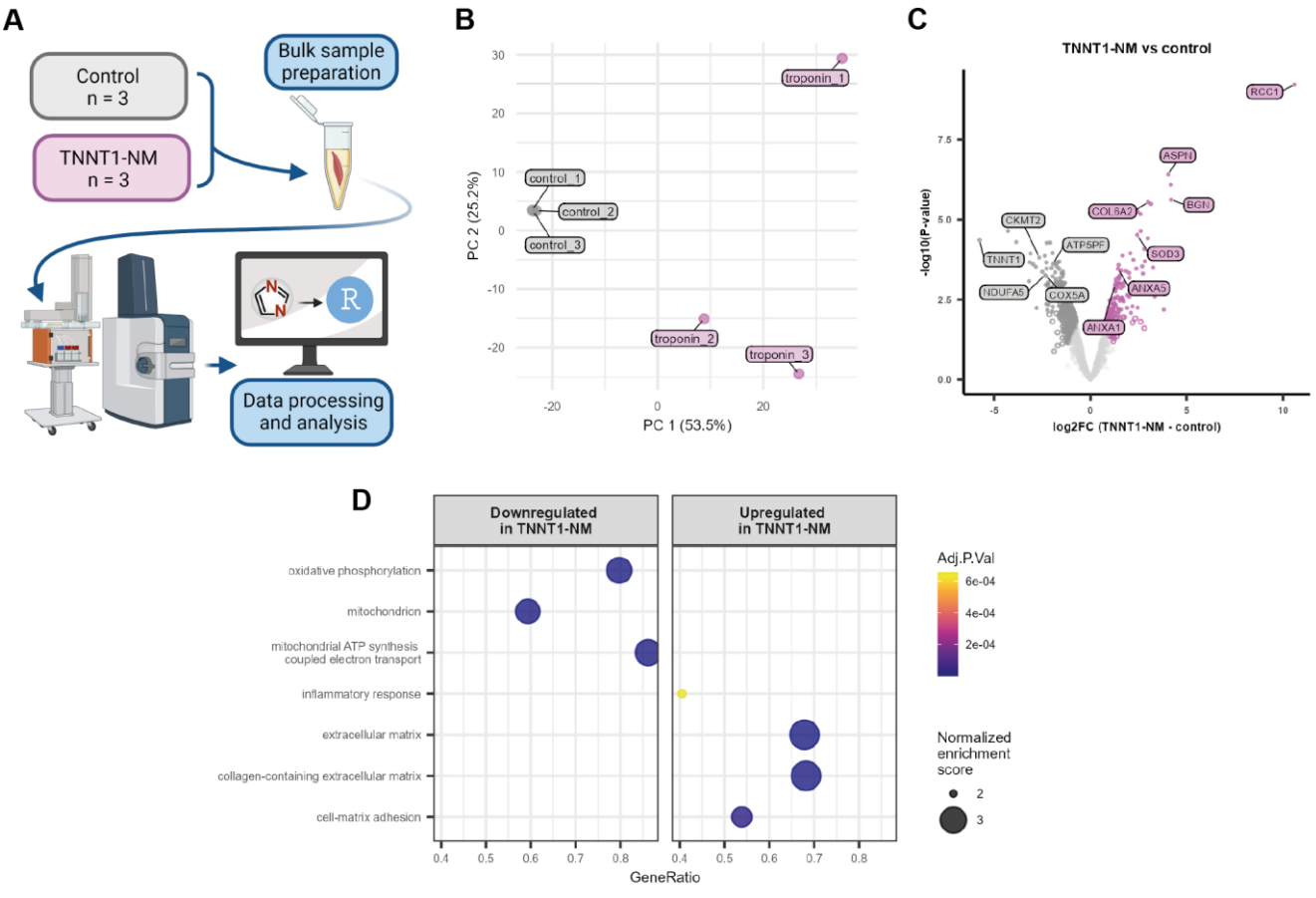

Supplementary Figure 13. Bulk muscle proteomics recapitulates single-fiber analysis of nemaline myopathy samples. (**A**) Workflow of bulk muscle proteomics for control participants and *TNNT1*-nemaline myopathy patients (created using BioRender.com). (**B**) Principal component analysis (PCA) plot of bulk skeletal muscle from *TNNT1*-nemaline myopathy patients and controls. **(C)** Volcano plot comparing the *TNNT1*-nemaline myopathy with control participants. Colored circles represent significantly different proteins at $\pi < 0.05$, darker dots represent significantly different proteins at FDR < 0.05. Statistical analysis was performed using a Limma linear model approach with empirical Bayes methods followed by p-value adjustment (Benjamini-Hochberg). **(D)** Enrichment analysis of significantly different proteins in the bulk muscle proteome between TNNT1-nemaline myopathy patients and control participants. Statistical analysis was performed using the clusterProfiler package with Benjamini-Hochberg adjusted p values.(n = 3 for each group).

Supplementary table 1. Characteristics of participants of the 1000 fiber transcriptomics and proteomics datasets.

	Transcriptomics	**Proteomics**
n	14 (12M 2F)	5 (5M)
Age (years)	28 ± 6	29 ± 5
Height (cm)	178 ± 8	184 ± 2
Weight (kg)	77.0 ± 17.2	93 ± 8.3
BMI (kg/m^2)	24.1 ± 4.0	27.6 ± 2.8
Maximal heart rate (beats/min)	192 ± 9	
Maximal oxygen uptake (L/min)	3.6 ± 0.7	4.2 ± 0.4
Maximal oxygen uptake (mL/min/kg)	49.7 ± 9.1	45.8 ± 0.6

Supplementary table 2. Classification system for fiber typing based on myosin heavy chain isoform expression.

MYH marker combination	Assigned MYH fiber type
MYH7+/MYH2-/MYH1-	Type 1
MYH7-/MYH2+/MYH1-	Type 2A
MYH7-/MYH2-/MYH1+	Type 2X
MYH7+/MYH2+/MYH1-	Hybrid 1/2A
MYH7-/MYH2+/MYH1+	Hybrid 2A/2X

Supplementary table 3. Characteristics of patients within the nemaline myopathy proteomics dataset.

Condition (Causal gene)	Age (y)	Sex	Pathogenic variant
Control	23	M	-
Control	22	M	-
Control	30	M	-
ACTA1	3	M	c.611C>T
ACTA1	13	M	c.487C>CG
ACTA1	11	F	c.158A>T
TNNT1	10 months	F	homozygous c.661G>T; p.E221X
TNNT1	1	F	homozygous c.505G>T
TNNT1	1	F	homozygous c.505G>T